ChemPubSoc Europe
DOI: 10.1002/cctc.201600123
CHEMCATCHEM
Full Papers

Role of Nitrogen Doping on the Performance of Carbon Nanotube Catalysts: A Catalytic Wet Peroxide Oxidation Application

Maria Martin-Martinez,[a] Rui S. Ribeiro,[a] Bruno F. Machado,[b] Philippe Serp,[b] Sergio Morales-Torres,[c] Adrián M. T. Silva,[c] José L. Figueiredo,[c] Joaquim L. Faria,[c] and Helder T. Gomes*[a]

Four magnetic carbon nanotube (CNT) samples (undoped, completely N-doped, and two selectively N-doped) were synthesized by chemical vapor deposition. The materials were tested in the catalytic wet peroxide oxidation (CWPO) of highly concentrated 4-nitrophenol solutions (4-NP, 5 gL^{-1}). Relatively mild operating conditions were considered (atmospheric pressure, $T=50\,^{\circ}C$, pH 3), using a catalyst load of 2.5 gL^{-1} and the stoichiometric amount of H_2O_2 needed for the complete mineralization of 4-NP. N-doping was identified to influence considerably the CWPO performance of the materials. In particular, undoped CNTs, with a moderate hydrophobicity, favor the controllable and efficient decomposition of H_2O_2 into highly reactive hydroxyl radicals ($HO^{\bullet}$), thus showing high catalytic activity for 4-NP degradation. On the other hand, the completely N-doped catalyst, fully hydrophilic, favors a quick decomposition of H_2O_2 into nonreactive O_2 and H_2O species. The selectively N-doped amphiphilic catalysts, that is, hybrid structures containing undoped sections followed by N-doped ones, provided intermediate results, namely, a higher N content favored H_2O_2 decomposition towards nonreactive H_2O and O_2 species, whereas a lower N content resulted in the formation of $HO^{\bullet}$, increasing 4-NP mineralization. Catalyst stability and reusability were also investigated by consecutive CWPO runs.

Introduction

During the past decade, the development and use of different nanostructured porous carbon materials in catalysis have increased in importance, with these carbon materials used as supports or as catalysts on their own.[1] Carbon nanotubes (CNTs) are particularly suitable for liquid-phase reactions, owing to their high external surface area.[2] In addition, they exhibit high mechanical resistance, superior electronic properties, relatively high thermal stability under oxidizing conditions, and tunable surface chemistry, making them highly versatile for several applications.[2] Moreover, the presence of nitrogen in the structure of CNTs increases their polarity and improves their reactivity towards different molecules.[3] In this sense, amphiphilic materials produced by selective N-doping are gaining interest for several applications.[4,5] Pioneering works have reported the synthesis of magnetic amphiphilic N-doped CNTs from a Fe/γ-Al_2O_3 catalyst and their successful application in different processes, such as adsorption of polyaromatic hydrocarbons,[3] chemical oxidation of alcohols,[3,6] and transesterification of soybean oil.[3] Moreover, it is known that the presence of N groups on the CNT surface highly enhances their activity for hydrogen peroxide (H_2O_2) decomposition.[7,8]

Advanced oxidation processes, primarily based on the action of hydroxyl radicals ($HO^{\bullet}$) to oxidize organic pollutants, are regarded as promising solutions for the treatment of aqueous effluents from pharmaceutical, petrochemical, dye, or paper industries, among others, containing recalcitrant and nonbiodegradable compounds[9,10] difficult to remove by conventional biological processes, mainly if present at high concentrations (1–10 gL^{-1}).[11] Among them, catalytic wet peroxide oxidation (CWPO) uses H_2O_2 as a source of $HO^{\bullet}$ and a suitable catalyst for the degradation of the organic species under relatively mild conditions (0.1–0.2 MPa and 20–130 °C).[12,13]

H_2O_2 easily decomposes into oxygen and water [Eq. (1)], releasing heat. Nevertheless, for the CWPO process, it is impor-

---

[a] Dr. M. Martin-Martinez, R. S. Ribeiro, Dr. H. T. Gomes
Laboratory of Separation and Reaction Engineering
- Laboratory of Catalysis and Materials (LSRE-LCM)
Departamento de Tecnologia Química e Biológica
Escola Superior de Tecnologia e Gestão
Instituto Politécnico de Bragança
Campus de Santa Apolónia, 5300-253 Bragança (Portugal)
E-mail: htgomes@ipb.pt

[b] Dr. B. F. Machado, Dr. P. Serp
Laboratoire de Chimie de Coordination UPR CNRS 8241
composante ENSIACET
Université de Toulouse
UPS-INP-LCC 4 allé Emile Monso BP 44362
31030 Toulouse Cedex 4 (France)

[c] Dr. S. Morales-Torres, Dr. A. M. T. Silva, Dr. J. L. Figueiredo, Dr. J. L. Faria
Laboratory of Separation and Reaction Engineering
- Laboratory of Catalysis and Materials (LSRE-LCM)
Departamento de Engenharia Química, Faculdade de Engenharia
Universidade do Porto
Rua Dr. Roberto Frias s/n, 4200-465 Porto (Portugal)

Supporting information and the ORCID identification number(s) for the author(s) of this article can be found under http://dx.doi.org/10.1002/cctc.201600123.

tant to decompose selectively H_2O_2 into highly reactive $HO^\bullet$. The reaction mechanisms describing H_2O_2 decomposition are well accepted and reported in the literature, including the formation of $HO^\bullet$ with the participation of a suitable catalyst, as shown in Equations (2–5) (in which [AS] refers to an adequate active site at the surface of the catalyst, for example, a surface-reducing active site or a transition-metal particle, among others).[14–20] However, radical recombination may also occur [Eqs. (6–8)], affecting the efficiency of the CWPO process.[15,21,22]

$$2\,H_2O_2 \rightarrow 2\,H_2O + O_2 \tag{1}$$

$$H_2O_2 + [AS] \rightarrow [AS^{\bullet+}] + OH^- + HO^\bullet \tag{2}$$

$$H_2O_2 + [AS^{\bullet+}] \rightarrow [AS] + H^+ + HOO^\bullet \tag{3}$$

$$H_2O_2 + HO^\bullet \rightarrow HOO^\bullet + H_2O \tag{4}$$

$$H_2O_2 + HOO^\bullet \rightarrow HO^\bullet + H_2O + O_2 \tag{5}$$

$$HO^\bullet + HO^\bullet \rightarrow H_2O_2 \tag{6}$$

$$HOO^\bullet + HOO^\bullet \rightarrow H_2O_2 + O_2 \tag{7}$$

$$HO^\bullet + HOO^\bullet \rightarrow H_2O + O_2 \tag{8}$$

The classical heterogeneous catalysts employed in CWPO consist of an active phase, mainly Fe or Cu, immobilized on the surface of a porous support (activated carbon, silica, pillared clays, or zeolites, among others). However, these catalysts usually suffer from severe deactivation resulting from leaching of the metallic phase after a few hours of operation.[23–27] Recently, metal-free carbon-based materials[28] were found to be promising catalysts for CWPO, showing high activity and stability and the ability to ensure an efficient H_2O_2 usage, that is, the selective formation of $HO^\bullet$ and further effective reaction with pollutant molecules.[14,29–31]

In previous studies,[32,33] the behavior of different commercial CNTs in the CWPO process was analyzed. These materials were found to be highly effective for the removal of different phenolic compounds, even without added metal species. As, to the best of our knowledge, amphiphilic CNTs have never been reported in CWPO, the present work aims to assess the role of N doping in CNTs if employed in CWPO. In addition, the presence of reminiscent Fe in their structures, resulting from the synthesis procedure, will make them very attractive for CWPO applications coupled with in situ magnetic separation systems for catalyst recovery. For this purpose, three different N-doped CNTs (with varying doping levels) and one undoped CNT sample were synthesized and characterized. A highly concentrated (5 $g\,L^{-1}$) 4-nitrophenol (4-NP) solution was considered as a model system to simulate high-loaded wastewaters, challenging conditions normally not considered in CWPO studies.[34–36]

Results and Discussion

Carbon nanotubes characterization

The transmission electron microscopy (TEM) results reported in previous studies,[3,6,37] included in Table 1, reveal that the introduction of nitrogen in the carbon structure induces an increase of the tube diameter and a decrease in the interstitial space between individual CNTs. Undoped E30 consists of very regular multiwalled CNTs with an average external diameter of approximately 8 nm and Fe particles encapsulated in the structure (formed during the synthesis by catalytic chemical vapor deposition, CVD, through reduction of the iron oxide using H_2 produced during the decomposition of the carbon sources at high temperature, and that remained in the CNT structure after the purification step with H_2SO_4—see the Experimental Section). The yield of the CVD process was 4.8 $g_C\,g_{cat}^{-1}$.[3] On the other hand, the completely N-doped A30, generated in a considerable lower yield (1.1 $g_C\,g_{cat}^{-1}$),[3] is characterized by a "bamboo-like" structure with larger diameters (≈14 nm). The selectively N-doped materials are hybrid structures containing both undoped and N-doped sections with intermediate diameters (Supporting Information, Figure S1).

Table 1. Textural properties (average tube diameter and interstitial spacing) of the CNTs, extracted from TEM micrographs and N_2 adsorption–desorption isotherms.

Catalyst	Tube diameter [nm][a]	Interstitial space [nm][a]	S_{BET} (±5) [$m^2\,g^{-1}$]	V_{pore} (±0.01) [$cm^3\,g^{-1}$]	V_{meso} (±0.01) [$cm^3\,g^{-1}$]
E30	8	30.0	275	1.92	1.72
E10 A20	9	21.9	214	1.49	1.26
E3 A27	n/a	n/a	196	1.31	1.22
A30	14	14.8	212	1.11	0.74

[a] Data from [6]. n/a: not available.

Analysis of the N_2 adsorption–desorption isotherms obtained with the different CNTs (Figure S2; Table 1) reveals the highest value of specific surface area (S_{BET}) for the undoped material (E30), consistent with the lower tube diameter and hollow nature of its structure. It should be noted the area available inside E30 (assuming some opened tubes), contrary to the doped CNTs where the bamboo-type structure prevents a significant adsorption inside the tubes. With regard to the N-doped nanotubes, despite their larger tube diameter, the S_{BET} of the completely N-doped material (A30) is similar to that obtained for the selectively N-doped CNTs (E10 A20 and E3 A27), which might be explained by the smaller interstitial space shown by A30. The mesopore and total pore volumes also decrease as the nitrogen content in the CNT increases, which could be explained by a more efficient packing of the CNTs caused by an excess hydrogen bonding between functional groups, leading to thicker bundles.[38,39] In all cases, the nitrogen uptake dramatically increased at high relative pressures leading to a soft hysteresis loop, which may be associated to capillary condensation in the mesoporous structure of the CNT bundles.[40,41] By comparing the obtained isotherms, a significant difference in the shape of the hysteresis loop and a shift towards lower relative pressures are recorded for the completely N-doped A30 material, indicating a less uniform pore size distribution in this sample as compared to the other CNTs.

The N-doped CNT structure is known to show several defects and the presence of nitrogen in the graphitic network induces a curvature of the tube graphitic layers.[42] XRD, thermogravimetric, and Raman analysis performed previously[3,6,37] support the well-organized carbon structure of E30, as opposed to the more defective and reactive carbon present in A30, because a significant increase of defects occurs if increasing the N content. Briefly, Raman spectra showed the presence of one first-order peak at approximately 1560 cm^{-1} (G-band) and three second-order features at approximately 1330 cm^{-1} (D-band), 2700 cm^{-1} (G-band), and 2940 cm^{-1} (combined D/G-bands). The higher the ratio between D and G band intensities (I_D/I_G), the more defective is the structure under study. This parameter decreases from 0.8 in A30 to 0.6 in E30. Concomitantly, XRD analysis showed a slight decrease of $d_{(002)}$ spacing with the nitrogen content, from 3.43 Å in E30 to 3.36 Å in A30.

X-ray photoelectron spectroscopy (XPS) results (Table 2) confirm the low amount of nitrogen-containing surface groups on the N-doped materials, because these are mainly building blocks for the internal N–C bonds. Nevertheless, as reported before,[3] the deconvolution of the N 1s region of the XPS spectra (Figure S3) shows the presence of pyridinic nitrogen (N6), pyrrolic nitrogen (N5), quaternary nitrogen (NQ), and nitrogen oxides (N-oxides) in the N-doped materials, strongly affecting the CNT reactivity by their electron-donating properties. Pyridinic nitrogen, present on the edge of graphite planes bonded to two carbon atoms, has a well-known basic character, slightly more basic than that shown by the pyrrolic nitrogen. Both structures contain a basic nitrogen atom with a lone pair of electrons to donate. On the other hand, the positive charge of the quaternary nitrogen, in which nitrogen is within a graphite plane and bonded to three carbon atoms, favors the electron transfer reactions in the CNT surface. The peak related to nitrogen oxides is also present in the O 1s region of the N-doped materials (Table 2; Figure S4). The O 1s deconvolution reveals the presence of oxygen-containing surface groups in the CNTs as well, which could be formed during the CNT purification step with H_2SO_4. Although present in small amounts, the electron-withdrawing properties of these surface acidic oxygen-containing groups may also affect the reactivity of the CNTs. As observed in Table 2, the amount of oxygen-containing surface groups increases with the N content, affecting the type of surface chemical functionalities. As the undoped and the selectively N-doped CNTs (E30 and E10 A20) present intermediate amounts of carbonyl/carboxylic acid groups (C=O) and phenol/ether groups (C–O), the materials with high N content (E3 A27 and A30) present carbonyl/carboxylic acid groups in their surface. This is in accordance with the potentiometric titration curves (Figure S5), because the completely N-doped sample exhibits a broadening of the buffering area, showing the highest amount of surface acidic groups (Table 3). On the other hand, in spite of its small concentration, the total Fe on the CNTs also seems to increase with the presence of N (Table 2), in accordance with the remaining bulk Fe content determined in a previous study, which decreases from approximately 5% in the N-doped A30 to approximately 2% in the undoped E30.[6]

Table 3. Concentration of surface acidic groups and contact angles determined for buckypapers prepared with different CNTs.

Catalyst	Acidic groups [mmol g^{-1}]	Contact angle [°]	
E30	0.146	60 ± 2	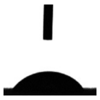
E10 A20	0.162	47 ± 2	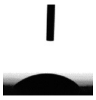
E3 A27	n.d.	16 ± 2	
A30	0.337	11 ± 1	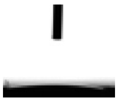

n.d.: not determined.

As explained above, both the undoped E30 and the completely N-doped A30 materials contain a single structure, consisting of very regular multiwalled CNTs in E30 and "bamboo-like" CNTs in A30. The thermogravimetric (TGA) curve (Figure 1) of the undoped E30 sample shows a maximum weight loss at 562.5 °C, which corresponds to the typical combustion temperature of multiwalled CNTs.[43] On the other hand, the completely N-doped A30 sample presented its maximum loss at a lower

Table 2. Surface atomic composition (by XPS) of the CNTs.

Catalyst	C [%]	O [%]	N [%]	Fe [%]	N 1s [%]				O 1s [%]		
					N6	N5	NQ	N-ox.	C=O	C–O	N-ox.
E30	99.0	0.85	–	0.05	–	–	–	–	46	54	–
E10 A20	98.9	0.75	0.29	0.06	37	17	26	20	46	51	3
E3 A27	94.9	1.6	3.4	0.2	33	6	27	34	58	29	13
A30	91.8	2.7	5.3	0.3	31	7	28	34	64	29	7

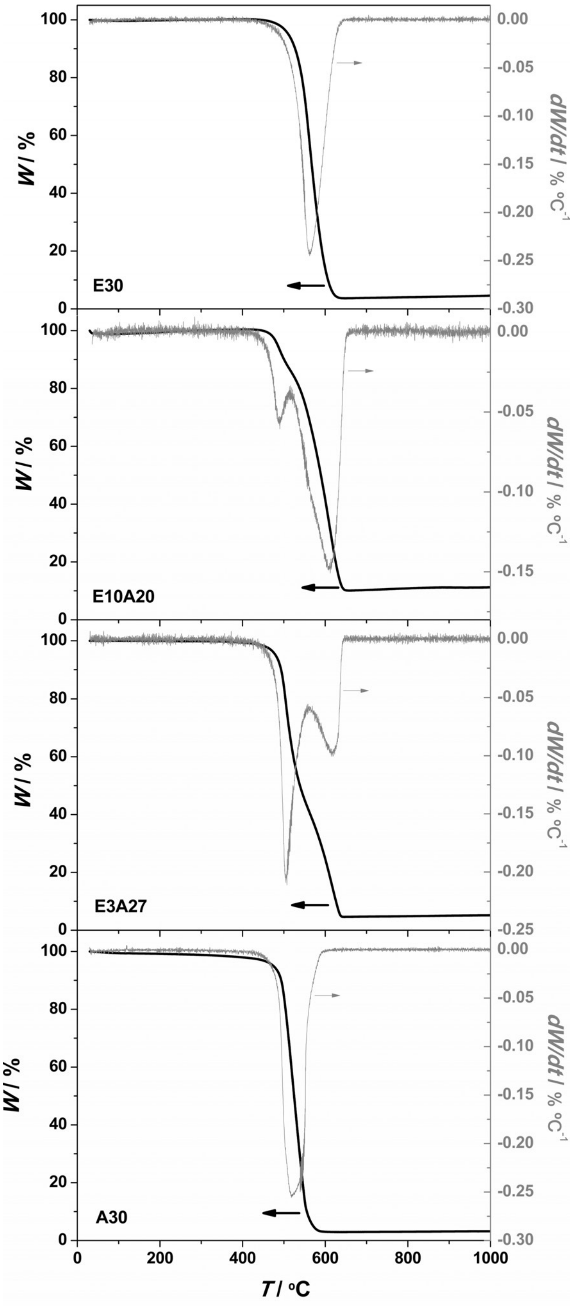

Figure 1. Weight loss by TGA of the CNTs (black) and their derivatives (gray).

temperature (539.2 °C), coherent with a more defective structure and the presence of oxygen- and nitrogen-containing surface groups. As pointed out by the TEM results, the TGA curves of the selectively N-doped CNTs confirm the presence of both structures in these materials, because two negative peaks situated at approximately 500 and 600 °C may be clearly identified in the weight-loss derivative (DTG curve), corresponding to N-doped and undoped sections, respectively.

Finally, the water contact-angle measurements obtained for the buckypapers composed of different CNTs (Table 3) seem to be correlated with the amount of oxygen- and nitrogen-containing functional groups incorporated during the CNT synthesis. In this context, the undoped material E30 has a moderate hydrophobicity (contact angle of 60°), and the N-doped catalysts are highly hydrophilic, in particular the completely N-doped A30 (contact angle of 11°). The hydrophilic properties and the N doping were found to strongly influence the activity and effectiveness of the CNTs if used as catalysts in the CWPO of 4-NP, as shown in the next section.

Catalytic activity

Screening experiments were performed to evaluate the performance of the synthesized CNTs during the CWPO of 4-NP. The conversions (*X*) of 4-NP, total organic carbon (TOC), and H_2O_2 achieved with each catalyst, as well as the concentration of Fe leached into the solution, after 24 h of reaction, are given in Figure 2. The removal of 4-NP in the absence of H_2O_2 is also shown in order to differentiate between pure adsorption and CWPO.

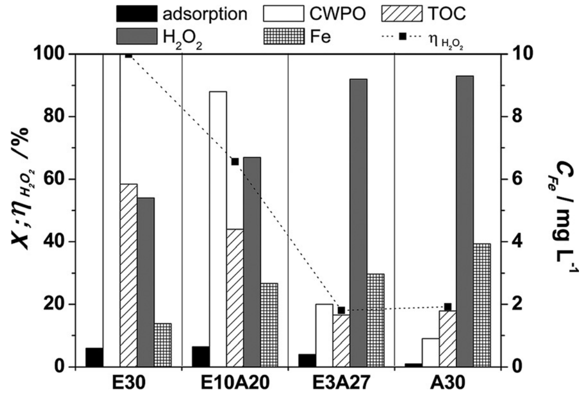

Figure 2. Removal of 4-NP from aqueous solution by adsorption and by CWPO; TOC removal, H_2O_2 decomposition, Fe leaching (right *y* axis) and $\eta_{H_2O_2}$ obtained in the CWPO experiments; results after 24 h.

As observed, the contribution of adsorption is negligible in all cases and decreases with increasing N content, presumably as a result of a weaker interaction with the N-doped surface. This enables the direct comparison of the different CNTs as catalysts in the CWPO experiments. All catalysts remarkably decompose H_2O_2, but with rather different catalytic activity. As expected, H_2O_2 consumption increases in the CNTs with higher amount of nitrogen,[7,8] because the presence of electron donating groups on these materials favors the decomposition of H_2O_2. However, contrary to expectations, 4-NP removal decreases with increasing H_2O_2 consumption; 100 % of the pollutant was removed after 24 h with the undoped material (E30), whereas only a 9 % removal was observed with the completely N-doped sample (A30). This singular behavior may be explained by the different physicochemical properties of the synthesized CNTs. In a previous study, it has been reported the ability of several carbon materials with different structural and chemical properties to selectively decompose H_2O_2 into $HO^{\bullet}$ radicals, revealing that the presence of basic groups in the carbon materials increases the yield of $HO^{\bullet}$ formation.[14] On the other hand, the hydrophilic N-doped catalysts have a strong affinity towards polar molecules such as H_2O_2. The insertion of N atoms in the CNT structure lowers the electron work function value of the carbonaceous surface, decreasing the band gap, thus producing a higher electron mobility and enhancing the decomposition of H_2O_2[44] into HO$^{\bullet}$ radicals, which ultimately result in the formation of nonreactive O_2 and H_2O species during the CWPO experiments. As explained in the Introduction, the formation of nonreactive species occurs in a two-step mechanism: first, H_2O_2 decomposes into reactive radicals, and second these radicals react between themselves, recombining into nonreactive species. Therefore, with the exception of E10 A20, very low 4-NP removal is reached by CWPO with the N-doped catalysts. On the other hand, the undoped E30 sample, which is moderately hydrophobic, has a modest affinity towards H_2O_2, resulting in a controllable and more efficient H_2O_2 decomposition into HO$^{\bullet}$, the first step in the CWPO process. These radicals further react with 4-NP adsorbed in the close vicinity of the active sites, resulting in a remarkable removal of 4-NP.

The different affinity of the CNTs for the reactant molecules (H_2O_2 and 4-NP) also affects the mineralization level obtained, the TOC conversion decreasing if using the CNTs with higher amount of nitrogen. Owing to a more efficient H_2O_2 decomposition into HO$^{\bullet}$, the undoped E30 catalyst converts approximately 60 % of the TOC content after 24 h. On the other hand, the inefficient decomposition of H_2O_2 into nonreactive species with the completely N-doped A30 hinders the reaction (TOC conversion of only approximately 18 %). This higher efficiency in the H_2O_2 decomposition with E30 is highlighted if analyzing the TOC removal per unit of H_2O_2 decomposed ($\eta_{H_2O_2}$). In this case, an efficiency of approximately 100 % is observed, suggesting that all the decomposed H_2O_2 is effectively used in the mineralization of 4-NP. In contrast, only approximately 20 % of the decomposed H_2O_2 was used in the mineralization of the pollutant with the highly N-doped E3 A27 material and the completely N-doped A30 sample.

Both the increase of structural defects in carbon materials[45,46] and presence of Fe at their surface[33,47] have been shown to increase the efficiency of CWPO processes, mainly related to increased H_2O_2 consumption. Nevertheless, if the sequence of the 4-NP removal obtained by CWPO in the presence of each catalyst (E30 > E10 A20 > E3 A27 > A30) is directly compared to that of the amount of surface Fe and defects in the structure of the catalysts (A30 > E3 A27 > E10 A20 > E30), an opposite tendency is observed. Therefore, surface Fe and structural defects cannot explain the results shown in Figure 2, suggesting that N-doping is a determining factor influencing the CNTs activity. The different textural properties observed for the CNTs could also have some influence on the catalyst activity. In particular, E30 is the most active material, with the highest S_{BET}, mesopore (V_{meso}), and total pore (V_{pore}) volumes, which could favor the accessibility of H_2O_2 to the active sites as well as 4-NP adsorption. However, these values are, in general, similar for all the samples, and the differences are only significant for E30. Therefore, it is possible to conclude that the influence of the N doping surpasses that of the textural properties of the CNTs.

In addition, the higher Fe leaching observed with the N-doped catalysts is in agreement with the higher content of Fe on the surface of the N-doped catalysts, and to the favorable conditions found at their surface for fast and inefficient H_2O_2 decomposition, resulting in the oxidation of the Fe particles and consequent leaching into the solution. Despite the higher amounts of leached Fe in the reactions with the N-doped catalysts, this factor does not lead to an increased 4-NP removal, discarding the homogeneous contribution promoted by Fe species in the solution. This further emphasizes the influence of N-doping on the efficiency of the CWPO process, as explained previously, by the different surface interactions between CNTs, H_2O_2, and 4-NP.

As explained above, the presence of electron-donating groups substantially favors the decomposition of H_2O_2. By studying the time evolution of 4-NP and H_2O_2 concentrations obtained with each catalyst during the CWPO runs (Figure 3), it can be observed that E30 and E10A20 decompose H_2O_2 at a moderate rate, but the highly and completely N-doped materials (E3 A27 and A30, respectively) promote a sharp decomposition of this oxidizing agent (also visually observed by the intense formation of gas bubbles and white smog in the reactor, pointing to the formation of O_2 and H_2O by recombination of the radicals).

To understand better the different behavior of the catalysts, the decomposition of H_2O_2 was studied without the presence of the pollutant. In Figure 4, the H_2O_2 concentration is shown as a function of time in the experiments conducted with and

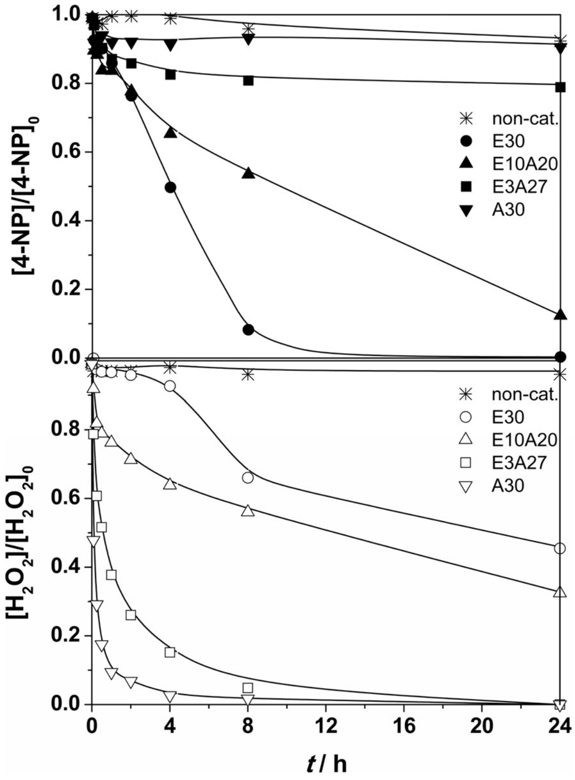

Figure 3. Concentration evolution with time (h) for 4-NP (top, solid symbols) and H_2O_2 (bottom, open symbols) during the CWPO experiments (normalized by the corresponding initial concentrations).

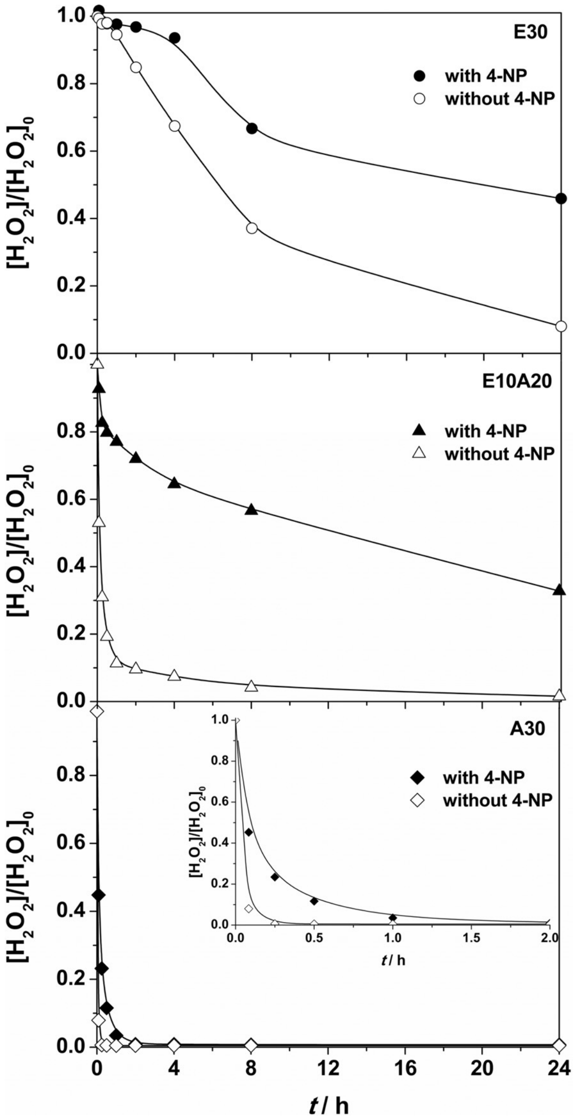

Figure 4. Concentration evolution with time (h) for H_2O_2 in experiments with (solid symbols) and without (open symbols) pollutant, using E30, E10 A20, and A30.

without 4-NP with three representative catalysts: the undoped E30 catalyst, the selectively N-doped E10 A20, and the completely N-doped A30. It is observed that the decomposition of H_2O_2 in the absence of 4-NP is faster in all cases, which may be explained by the absence of adsorption competition between H_2O_2 and 4-NP molecules on the surface of the catalyst. A noteworthy large difference is found in the catalyst E10 A20 with and without 4-NP, revealing that the competition between H_2O_2 and 4-NP for the catalyst surface hindered the strong affinity of H_2O_2 for the CNTs, resulting in a gradual decomposition of this reactant during the CWPO of 4-NP.

Reaction mechanism

To correlate the CWPO reaction mechanism with the different physicochemical properties of the synthesized CNTs, a more detailed study was performed with the three representative catalysts: E30, E10 A20, and A30. As observed in Figure 2, complete TOC conversion was never achieved with any of the catalysts, suggesting the existence of organic intermediates and/or byproducts at the end of the reaction. Accordingly, the time-evolution of the different compounds that were identified during the CWPO of 4-NP with E30, E10A20, and A30, is shown in Figure 5–7, respectively. As expected, the evolution of the identified compounds is quite different with each catalyst.

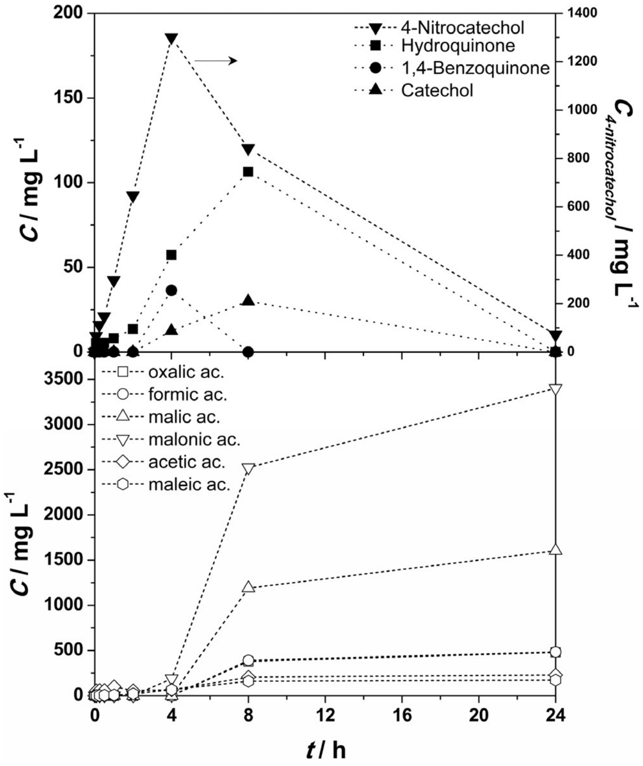

Figure 5. Concentration (mg L^{-1}) evolution with time (h) for the different compounds resulting from the CWPO of 4-NP using E30.

The first difference is related with the total concentration of intermediates and/or by-products obtained. The fast H_2O_2 consumption compared to 4-NP adsorption/decomposition, if using A30, limits the CWPO process. Therefore, small amounts of these compounds were detected with A30. Specifically, intermediate compounds were mainly formed during the first 2 h of reaction, during which H_2O_2 was still present in the solution. As described in a previous study,[45] the electrophilic addition of HO$^\bullet$ to the aromatic ring of 4-NP favors the formation of 4-nitrocatechol, which was by far the main aromatic compound formed with all the catalysts. However, secondary reactions also occur: 1) the denitration of the 4-NP molecule leading to the formation of hydroquinone, which may be further oxidized to 1,4-benzoquinone;[45,48] 2) the electrophilic HO$^\bullet$ addition at the *ortho* position leading to the formation of catechol. This is consistent with the aromatic intermediates observed with the undoped E30 catalyst (Figure 5). In this case, the concentrations observed follow the sequence: 4-nitrocatechol $>>>$ hydroquinone $>$ 1,4-benzoquinone $\approx$ catechol. On

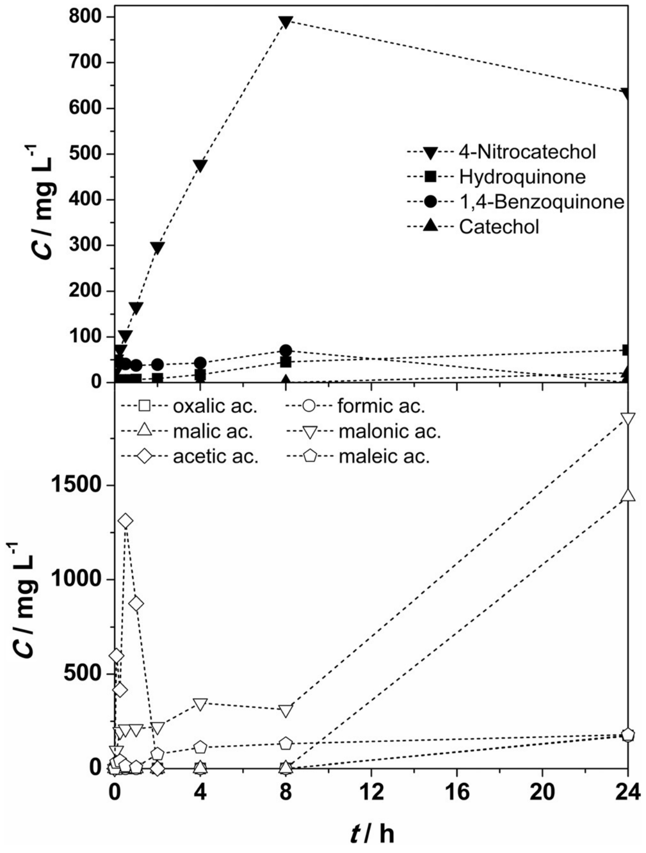

Figure 6. Concentration (mg L^{-1}) evolution with time (h) for the different compounds resulting from the CWPO of 4-NP using E10 A20.

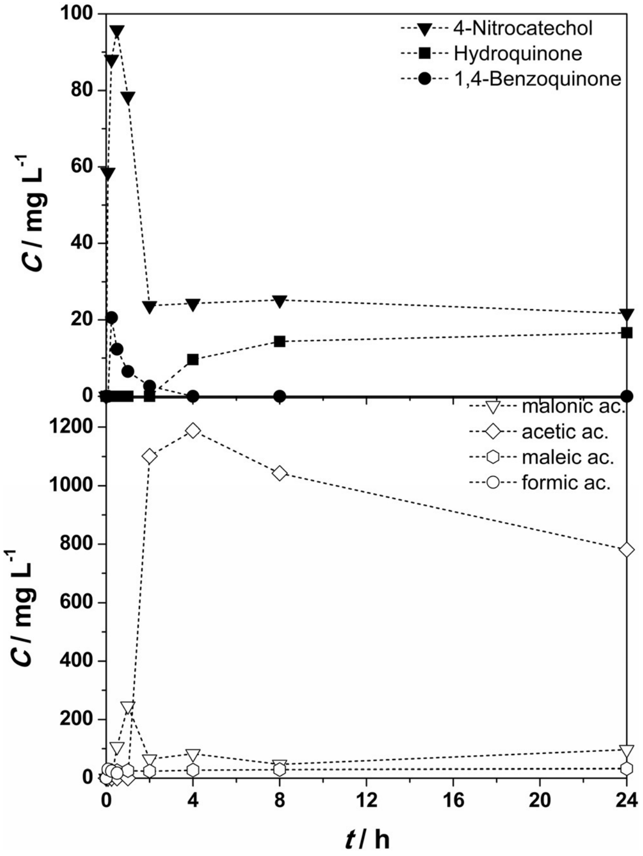

Figure 7. Concentration (mg L^{-1}) evolution with time (h) for the different compounds resulting from the CWPO of 4-NP using A30.

the other hand, with the completely N-doped A30 catalyst (Figure 7), the reaction medium was remarkably oxidizing as a result of the strong affinity between the catalysts and H_2O_2, and 1,4-benzoquinone was rapidly obtained. After about 2 h of reaction, H_2O_2 was completely consumed and 1,4-benzoquinone was immediately reduced back to hydroquinone, showing an atypical behavior in CWPO reactions.

As reported in previous studies,[32,45] HO$^\bullet$ radicals further attack these aromatic intermediates leading to the ring opening, and yielding low-molecular-weight carboxylic acids. With the undoped E30 catalyst (Figure 5), the aromatic intermediates were almost completely converted after 24 h of reaction and high concentrations of carboxylic acids were obtained, causing a dramatic decrease in the solution pH at the end of the reaction (dropping from 3 to 1.8). With the N-doped A30 sample (Figure 7), as explained above, the reaction environment in the first hours of reaction helped to highly oxidize 4-NP, forming considerable amounts of acetic acid, which decreased again when the reaction medium switch to a nonoxidizing environment. The E10 A20 catalyst behaved like A30 during the first minutes of reaction (Figure 6), with large amounts of acetic acid formed. However, after that, owing to the competition between H_2O_2 and 4-NP adsorption on the catalyst surface, the remaining H_2O_2 decomposed gradually and efficiently into HO$^\bullet$, switching to the undoped material-like behavior.

All the findings reported so far contribute to understand further the 4-NP CWPO mechanism if applying catalysts with different properties, as represented in Figure 8. The hydrophilic N-doped surfaces strongly attract the H_2O_2 molecules, which are quickly decomposed into radicals on the active sites with N-containing functionalities, owing to their electron-donating properties. The organic pollutant molecules cannot compete with H_2O_2 for the catalyst surface. Consequently, in a second

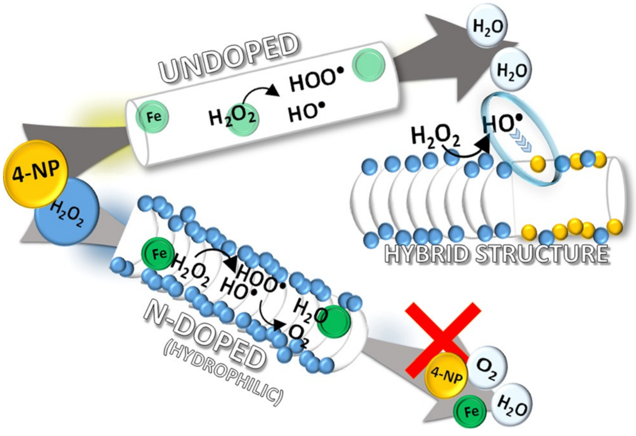

Figure 8. Proposed mechanism for the CWPO of 4-NP in N-doped hydrophilic and undoped catalyst surfaces.

stage, the radicals formed in large amounts do not react with the pollutant, but between themselves, recombining into nonreactive O_2 and H_2O. The more hydrophobic undoped surfaces attract both H_2O_2 and pollutant molecules. H_2O_2 is decomposed into radicals, which immediately attack the pollutant molecules adsorbed in the close vicinity, leading to their efficient mineralization. The hydrophilic N-doped sections in the hybrid structure strongly attract the H_2O_2 molecules. However, in this case, the pollutant molecule can approach the undoped sections and reach the catalyst surface, reacting with the formed radicals. This mechanistic insight puts into evidence amphiphilic materials as promising catalysts for CWPO.

The higher or lower hydrophilicity of the catalyst is directly affected by the N content. Then, if representing the 4-NP conversion obtained by CWPO, TOC removal, H_2O_2 conversion or $\eta_{H_2O_2}$ efficiency versus the catalyst contact angle (Figure 9), the higher H_2O_2 decomposition obtained on the highly hydrophilic surfaces of the completely N-doped CNTs is evidenced, but the 4-NP and TOC conversions are lower because of the poor efficiency of H_2O_2 decomposition, which forms nonreactive species.

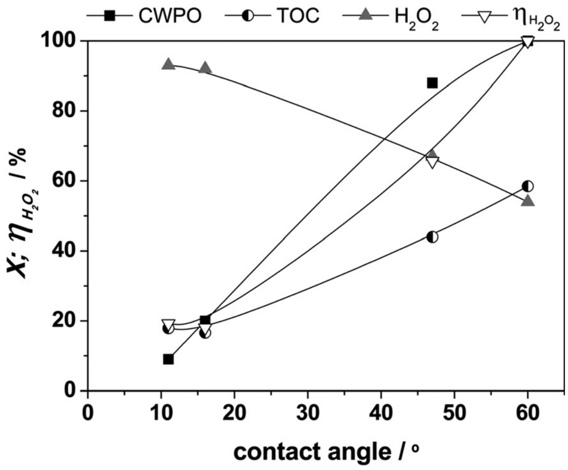

Figure 9. Conversion of 4-NP, TOC removal, H_2O_2 decomposition, and $\eta_{H_2O_2}$ (in %) obtained for the CWPO experiments after 24 h as a function of the catalyst contact angle (°).

Catalyst stability and reusability

An essential requirement for the industrial application of catalysts is their stability. To assess the stability and reusability properties, three consecutive CWPO runs were performed with the undoped E30 sample, which is the catalyst showing the best performance. As mentioned in the experimental section, the catalyst was recovered, washed with distilled water, and dried after each run, prior to its reuse in a new CWPO experiment. In Figure 10, the time evolution of the 4-NP concentration is shown during 24 h of reaction for the three consecutive CWPO cycles. Approximately 100 % of the initial pollutant was removed in the first and second cycles after 24 h of reaction. In the third run, however, the 4-NP conversion decreased, and approximately 30 h were needed to achieve total pollutant removal (results not shown). With the highly oxidizing reaction environment, the surface chemistry of E30 may change during the CWPO, turning it into a more hydrophilic structure, hindering its use in the consecutive reactions. Additional studies are needed to understand the catalyst performance and to identify the reasons for this behavior. Nevertheless, TEM images of the catalysts after CWPO are shown in Figure S6, and their comparison with the catalysts before CWPO (Figure S1) reveals no particular changes in the morphology of the materials during reaction.

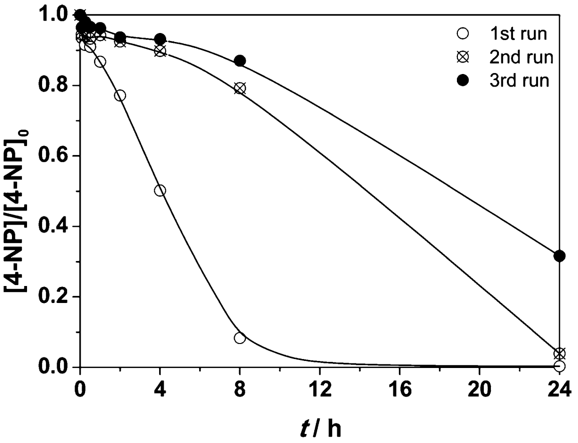

Figure 10. Concentration (normalized by the initial value) evolution with time (h) for 4-NP during three consecutive CWPO experiments using E30.

Considering the potential of amphiphilic CNTs in CWPO, the mechanisms involved in the deactivation of these materials are currently under study for further process improvement, as well as its possible optimization by intensification of the operating conditions and the production of more resistant materials against possible chemical alterations during the CWPO process.

Conclusions

Nitrogen doping of magnetic carbon nanotubes (CNTs) play a very important role in the catalytic wet peroxide oxidation (CWPO) performance of 4-nitrophenol (4-NP). Specifically, it affects the mechanism of H_2O_2 decomposition. The controllable H_2O_2 decomposition over hydrophobic undoped surfaces favors the formation of reactive $HO^\bullet$. On the other hand, the hydrophilic N-doped surfaces promote the total H_2O_2 decomposition into nonreactive species (H_2O and O_2). The competition between H_2O_2 and 4-NP for the catalyst surface in amphiphilic CNTs makes them promising catalysts for CWPO, because their combined hydrophilic N-doped sections (with high affinity for polar molecules) with undoped sections (ensuring a controllable and effective H_2O_2 decomposition) allow them to be explored in wastewater treatment.

Experimental Section

Chemicals

The main reactants involved in the process under study, 4-NP (98 wt %) and H_2O_2 (30 %, w/v), were purchased from Acros Organics and Fluka, respectively. Working standard solutions of formic acid (98 wt. %; Panreac), acetic acid (glacial acetic acid, 99.8 wt %; Fisher Chemical), oxalic acid, malonic acid, maleic acid, malic acid, hydroquinone, phenol (all 99 wt. %; Sigma–Aldrich), 1,4-benzoquinone (99.5 wt. %; Fluka), catechol (98 wt %; Fluka) and 4-nitrocatechol (98 wt. %; Fluka) were prepared and used for calibration in HPLC. Methanol (HPLC grade, 99.99 wt. %; Fisher Chemical), glacial acetic acid (HPLC grade, 99.99 wt. %; Fisher Chemical), acetonitrile (HPLC grade, 99.99 wt %; Fisher Chemical) and sulfuric acid (H_2SO_4, 96–98 wt %; Riedel-de-Haën) were used to prepare the mobile phases required for HPLC. The reactants used for the determination of Fe were L-ascorbic acid (99 wt %; Fisher Chemical), *o*-phenanthroline (99 wt. %; Panreac), glacial acetic acid (HPLC grade, 99.99 wt. %; Fisher Chemical), ammonium acetate (98 wt. %; Pronalab) and iron(II) chloride tetrahydrate (99 wt %; Sigma–Aldrich). Other reactants used were sodium hydroxide (NaOH, 98 wt %; Panreac), hydrochloric acid (HCl, 37 wt. %; Sigma–Aldrich), potassium nitrate (KNO_3, 99 wt. %; Sigma–Aldrich), titanium(IV) oxysulfate (15 wt. % in dilute sulfuric acid, 99.99 %; Sigma–Aldrich), and sodium sulfite (Na_2SO_3, 98 wt. %; Sigma–Aldrich). All chemicals were used as received without further purification. Distilled water was used throughout the work except for mobile phase preparation, for which ultrapure water was employed.

Synthesis of carbon nanotubes

The CNTs were synthesized by a catalytic CVD process in a fluidized-bed reactor, as described elsewhere,[3] using ethylene as a carbon source and acetonitrile/N_2 as a carbon/nitrogen source, at 650 °C. The synthesis was conducted in the presence of a Fe/γ-Al_2O_3 (20 wt. % Fe) catalyst prepared by impregnation and reduced in situ at 650 °C for 30 min. Four samples were produced by feeding to the fluidized bed reactor: 1) ethylene alone for 30 min (sample E30); 2) ethylene for 10 min, followed by acetonitrile/N_2 for 20 min (sample E10 A20); 3) ethylene for 3 min, followed by acetonitrile/N_2 for 27 min (sample E3 A27); and 4) acetonitrile/N_2 alone for 30 min (sample A30). Finally, the synthesized CNTs were purified under reflux at 140 °C, with an aqueous solution of H_2SO_4 (50 vol. %) for 3 h to facilitate the total dissolution of the alumina and exposed Fe particles.

Characterization of the carbon nanotubes

N_2 adsorption–desorption isotherms (−196 °C) were obtained to characterize the textural properties of the materials (Quantachrome autosorb-iQ2). The samples were previously outgassed for 12 h at 120 °C. The S_{BET} was calculated by the BET equation,[49] and the V_{meso} and V_{pore} volumes were estimated using the BJH method.[50] The surface chemical composition of the CNTs was analyzed by XPS (Kratos AXIS Ultra HSA spectrometer), using MgK_α radiation (1486.7 eV). The elements present and their corresponding concentrations were determined by recording general XPS spectra, scanning up to a binding energy (BE) of 1300 eV. The C 1s peak (284.9 eV) was taken as an internal standard to correct the shift in BE caused by sample charging. The BE of the C 1s, N 1s, O 1s and Fe 2$p_{3/2}$ core levels and the full width at half maximum values were used to assess the chemical state of these elements on the catalyst surface, according to NIST database. Potentiometric titration (Metrohm 670 automatic titrator) was used to estimate the concentration of acidic active sites at the catalysts surface. CNTs (50 mg) dispersed in a 25 mL volume of aqueous HCl (0.0070 mol L^{-1}) and KNO_3 (0.04 mol L^{-1}) solutions were placed directly into the electrochemical cell and titrated with a CO_2-free NaOH solution (0.0524 mol L^{-1}). The experimental data were treated according to the literature.[51,52] TGA analyses were performed by using an Elmer Diamond TG/DTA thermo balance, heating the sample powders at 10 °C min^{-1} up to 1000 °C in air atmosphere (50 cm^3 min^{-1}). The hydrophobicity/hydrophilicity of the CNTs (in the form of buckypapers) was determined by water contact-angle measurements using an Attension optical tensiometer (model Theta) that allowed image acquisition and data analysis. The measurements with water were performed on dry buckypapers at RT using the sessile-drop method.[38] Each contact angle was measured at least in five different locations on the buckypapers to determine the average value. TEM images were obtained by using a TEM-FEI microscope (Tecnai-G2-20-FEI 2006) operating at 200 kV. The samples magnetism was verified qualitatively by using magnets (Figure S7).

CWPO, adsorption, and H_2O_2 decomposition experiments

The CWPO runs were conducted in a batch reaction system consisting of a 250 mL magnetically stirred (600 rpm) glass reactor, equipped with a reflux condenser and a sample collection port, immersed in an oil bath with temperature control. In a typical experiment, the reactor was loaded with a 50 mL volume of the 4-NP aqueous solution (5 g L^{-1}) and heated up to 50 °C. After temperature stabilization, pH was adjusted to 3 by using H_2SO_4 and NaOH solutions, and a calculated volume of H_2O_2 was incorporated to the system to reach the stoichiometric concentration needed to mineralize completely 4-NP. The reaction started with the addition of the catalyst (0.125 g) corresponding to a catalyst load of 2.5 g L^{-1}. During the experiment, samples of the resulting effluent were collected at different reaction times (typically at 0, 5, 15, 30, 60, 120, 240, 480, and 1440 min) and prepared for analysis, as described below. After 24 h of reaction, the catalyst was separated by filtration (20 μm, Prat Dumas), washed with distilled water and dried at 60 °C. A blank experiment, that is, without catalyst, was performed to assess possible noncatalytic oxidation reactions promoted by H_2O_2. On the other hand, the adsorption capacity of the different synthesized CNTs was evaluated by means of pure adsorption experiments, in which the operating conditions used in the CWPO runs were reproduced, but a volume of distilled water was incorporated to the system in substitution of H_2O_2. Finally, to assess the activity of the catalysts to decompose H_2O_2 avoiding pollutant competition, a set of experiments was conducted by introducing distilled water (50 mL) in the reactor instead of the 4-NP aqueous solution. The experiments were performed in triplicate, the standard deviation was less than 5 % in all cases.

Analytical methods

4-NP and the aromatic intermediates derived from its oxidation were identified and quantified by HPLC, adapting the procedure described elsewhere,[53] using a Jasco system equipped with an UV/Vis detector (UV-2075 Plus) and a quaternary gradient pump (PU-2089 Plus) for solvent delivery (1 mL min^{-1}). The stationary phase consisted of a Kromasil 100-5-C18 column (15 cm × 4.6 mm; 5 μm particle size) working at RT. As explained above, small aliquots were periodically withdrawn from the reactor. An excess of Na_2SO_3 was immediately added to consume the residual H_2O_2 and the catalyst was removed by filtration to stop the reaction.[33,36,54] The mobile phase consisted of an isocratic method of an A:B (40:60) mixture of 3% acetic acid and 1% acetonitrile in methanol (A) and 3% acetic acid in ultrapure water (B). The absorbance wavelength was adjusted to 318 nm for the determination of 4-NP, and to 277 nm for the aromatic intermediates. The concentration of carboxylic acids was monitored by a Jasco HPLC system fitted with an YMC-Triart C18 column (25 cm×4.6 mm; 5 μm particle size), adapting the procedures reported elsewhere.[55,56] The mobile phase consisted of an isocratic method of an A:B (95:5) mixture of 1% sulfuric acid in ultrapure water (A) and acetonitrile (B), delivered to the system at 0.6 mL min^{-1}. The UV/Vis detector was set to 210 nm. The TOC content and the concentration of nitrate ions were determined using a Shimadzu TOC-5000A analyzer and a Metrohm 881 Compact Ion Chromatograph equipped with a Metrosep A Supp 7-250 column, respectively. The concentrations of H_2O_2 and Fe in solution were determined by colorimetric methods with a UV/Vis spectrophotometer (T70 spectrometer, PG Instruments Ltd.). For the determination of H_2O_2, a filtered sample was acidified with a H_2SO_4 0.5 M solution. 0.1 mL of titanium oxysulfate was added, and the absorbance was measured at 405 nm.[57] On the other hand, the concentration of Fe species leached at the end of the experiments was determined by the *o*-phenanthroline method, according to ISO 6332,[58] using ascorbic acid as reducing agent, and measuring the absorbance at 510 nm.

Acknowledgements

This work was co-financed by FCT and FEDER under Programme PT2020 (Project UID/EQU/50020/2013) and Programme COMPETE (FCOMP-01-0124-FEDER-020706), and by QREN, ON2, FCT and FEDER (Project NORTE-07-0124-FEDER-000015). M. Martin-Martinez (Postdoc grant SFRH/BPD/108510/2015), R.S. Ribeiro (Ph.D. grant SFRH/BD/94177/2013, co-financed by FCT and the European Social Fund through POPH and QREN), S. Morales-Torres (Postdoc grant SFRH/BPD/108981/2015) and A.M.T. Silva (FCT Investigator 2013 Programme IF/01501/2013) acknowledge financial support from the FCT.

Keywords: doping · environmental chemistry · heterogeneous catalysis · nanotubes · nitrogen · oxidation

[1] P. Zhang, H. Zhu, S. Dai, *ChemCatChem* **2015**, *7*, 2788 – 2805.
[2] P. Serp, M. Corrias, P. Kalck, *Appl. Catal. A* **2003**, *253*, 337 – 358.
[3] A. D. Purceno, B. F. Machado, A. P. C. Teixeira, T. V. Medeiros, A. Benyounes, J. Beausoleil, H. C. Menezes, Z. L. Cardeal, R. M. Lago, P. Serp, *Nanoscale* **2015**, *7*, 294 – 300.
[4] M. Pera-Titus, L. Leclercq, J. Clacens, F. De Campo, V. Nardello-Rataj, *Angew. Chem. Int. Ed.* **2015**, *54*, 2006 – 2021; *Angew. Chem.* **2015**, *127*, 2028 – 2044.
[5] Y. Yang, W. Zhang, X. Ma, H. Zhao, X. Zhang, *ChemCatChem* **2015**, *7*, 3454 – 3459.
[6] A. Benyounes, S. Louisia, R. Axet, Z. Mahfoud, M. Kacimi, P. Serp, *Catal. Today* **2015**, *249*, 137 – 144.
[7] K. V. Voitko, R. L. D. Whitby, V. M. Gun'ko, O. M. Bakalinska, M. T. Kartel, K. Laszlo, A. B. Cundy, S. V. Mikhalovsky, *J. Colloid Interface Sci.* **2011**, *361*, 129 – 136.
[8] K. Voitko, A. Tóth, E. Demianenko, G. Dobos, B. Berke, O. Bakalinska, A. Grebenyuk, E. Tombácz, V. Kuts, Y. Tarasenko, M. Kartel, K. László, *J. Colloid Interface Sci.* **2015**, *437*, 283 – 290.
[9] R. Andreozzi, V. Caprio, A. Insola, R. Marotta, *Catal. Today* **1999**, *53*, 51 – 59.
[10] G. Pliego, J. A. Zazo, P. Garcia-Munoz, M. Munoz, J. A. Casas, J. J. Rodriguez, *Crit. Rev. Environ. Sci. Technol.* **2015**, *45*, 2611 – 2692.
[11] S. Azabou, W. Najjar, M. Bouaziz, A. Ghorbel, S. Sayadi, *J. Hazard. Mater.* **2010**, *183*, 62 – 69.
[12] S. Navalon, A. Dhakshinamoorthy, M. Alvaro, H. Garcia, *ChemSusChem* **2011**, *4*, 1712 – 1730.
[13] C. W. Jones, *Applications of hydrogen peroxide and derivatives*, Royal Society of Chemistry, **1999**.
[14] R. S. Ribeiro, A. M. T. Silva, J. L. Figueiredo, J. L. Faria, H. T. Gomes, *Carbon* **2013**, *62*, 97 – 108.
[15] G. V. Buxton, C. L. Greenstock, W. P. Helman, A. B. Ross, *J. Phys. Chem. Ref. Data* **1988**, *17*, 513 – 886.
[16] W. H. Koppenol, J. Butler, J. W. v. Leeuwen, *Photochem. Photobiol.* **1978**, *28*, 655 – 658.
[17] S. Ghafoori, M. Mehrvar, P. K. Chan, *Ind. Eng. Chem. Res.* **2012**, *51*, 14980 – 14993.
[18] T. Schaefer, J. Schindelka, D. Hoffmann, H. Herrmann, *J. Phys. Chem. A* **2012**, *116*, 6317 – 6326.
[19] A. Rey, A. Bahamonde, J. A. Casas, J. J. Rodriguez, *Water Sci. Technol.* **2010**, *61*, 2769 – 2778.
[20] A. Aguinaco, J. P. Pocostales, J. Garcia-Araya, F. J. Beltran, *J. Chem. Technol. Biotechnol.* **2011**, *86*, 595 – 600.
[21] B. H. J. Bielski, D. E. Cabelli, R. L. Arudi, A. B. Ross, *J. Phys. Chem. Ref. Data* **1985**, *14*, 1041 – 1100.
[22] A. J. Elliot, G. V. Buxton, *J. Chem. Soc. Faraday Trans.* **1992**, *88*, 2465 – 2470.
[23] E. V. Rokhina, J. Virkutyte, *Crit. Rev. Environ. Sci. Technol.* **2010**, *41*, 125 – 167.
[24] G. Calleja, J. A. Melero, F. Martinez, R. Molina, *Water Res.* **2005**, *39*, 1741 – 1750.
[25] A. Rey, M. Faraldos, J. A. Casas, J. A. Zazo, A. Bahamonde, J. J. Rodriguez, *Appl. Catal. B* **2009**, *86*, 69 – 77.
[26] A. Onda, Y. Suzuki, S. Takemasa, K. Kajiyoshi, K. Yanagisawa, *J. Mater. Sci.* **2008**, *43*, 4230 – 4235.
[27] F. Martínez, J. A. Melero, J. A. Botas, M. I. Pariente, R. Molina, *Ind. Eng. Chem. Res.* **2007**, *46*, 4396 – 4405.
[28] L. Liu, Y. Zhu, M. Su, Z. Yuan, *ChemCatChem* **2015**, *7*, 2765 – 2787.
[29] R. S. Ribeiro, A. M. T. Silva, M. T. Pinho, J. L. Figueiredo, J. L. Faria, H. T. Gomes, *Catal. Today* **2015**, *240*, 61 – 66.
[30] *Carbon Materials for Catalysis* (Eds.: P. Serp, J. L. Figueiredo), Wiley, **2009**.
[31] C. M. Domínguez, P. Ocón, A. Quintanilla, J. A. Casas, J. J. Rodriguez, *Appl. Catal. B* **2013**, *140 – 141*, 663 – 670.
[32] M. T. Pinho, H. T. Gomes, R. S. Ribeiro, J. L. Faria, A. M. T. Silva, *Appl. Catal. B* **2015**, *165*, 706 – 714.
[33] R. S. Ribeiro, A. M. T. Silva, J. L. Figueiredo, J. L. Faria, H. T. Gomes, *Appl. Catal. B* **2013**, *140 – 141*, 356 – 362.
[34] W. Liu, J. Qian, K. Wang, H. Xu, D. Jiang, Q. Liu, X. Yang, H. Li, *J. Inorg. Organomet. Polym. Mater.* **2013**, *23*, 907 – 916.
[35] F. Martínez, M. I. Pariente, J. Á. Botas, J. A. Melero, A. Rubalcaba, *J. Chem. Technol. Biotechnol.* **2012**, *87*, 880 – 886.
[36] F. Duarte, F. J. Maldonado-Hódar, L. M. Madeira, *Appl. Catal. B* **2011**, *103*, 109 – 115.
[37] H. C. Menezes, S. M. R. de Barcelos, D. F. D. Macedo, A. D. Purceno, B. F. Machado, A. P. C. Teixeira, R. M. Lago, P. Serp, Z. L. Cardeal, *Anal. Chim. Acta* **2015**, *873*, 51 – 56.
[38] S. Morales-Torres, T. L. S. Silva, L. Pastrana-Martinez, A. T. S. C. Brandao, J. L. Figueiredo, A. M. T. Silva, *Phys. Chem. Chem. Phys.* **2014**, *16*, 12237 – 12250.
[39] G. E. Romanos, V. Likodimos, R. R. N. Marques, T. A. Steriotis, S. K. Papageorgiou, J. L. Faria, J. L. Figueiredo, A. M. T. Silva, P. Falaras, *J. Phys. Chem. C* **2011**, *115*, 8534 – 8546.
[40] M. Soria-Sánchez, E. Castillejos-López, A. Maroto-Valiente, M. F. R. Pereira, J. J. M. Órfão, A. Guerrero-Ruiz, *Appl. Catal. B* **2012**, *121 – 122*, 182 – 189.
[41] Q. Yang, P. Hou, S. Bai, M. Wang, H. Cheng, *Chem. Phys. Lett.* **2001**, *345*, 18 – 24.
[42] A. A. Koós, M. Dowling, K. Jurkschat, A. Crossley, N. Grobert, *Carbon* **2009**, *47*, 30 – 37.
[43] D. Bom, R. Andrews, D. Jacques, J. Anthony, B. Chen, M. S. Meier, J. P. Selegue, *Nano Lett.* **2002**, *2*, 615 – 619.

[44] V. V. Strelko, V. S. Kuts, P. A. Thrower, *Carbon* **2000**, *38*, 1499–1503.
[45] R. S. Ribeiro, A. M. T. Silva, L. Pastrana-Martinez, J. L. Figueiredo, J. L. Faria, H. T. Gomes, *Catal. Today* **2015**, *249*, 204–212.
[46] A. Rey, J. A. Zazo, J. A. Casas, A. Bahamonde, J. J. Rodriguez, *Appl. Catal. A* **2011**, *402*, 146–155.
[47] C. M. Domínguez, A. Quintanilla, P. Ocón, J. A. Casas, J. J. Rodriguez, *Carbon* **2013**, *60*, 76–83.
[48] M. A. Oturan, J. Peiroten, P. Chartrin, A. J. Acher, *Environ. Sci. Technol.* **2000**, *34*, 3474–3479.
[49] S. Brunauer, P. H. Emmett, E. Teller, *J. Am. Chem. Soc.* **1938**, *60*, 309–319.
[50] E. P. Barrett, L. G. Joyner, P. P. Halenda, *J. Am. Chem. Soc.* **1951**, *73*, 373–380.
[51] J. P. de Mesquita, P. B. Martelli, H. d. F. Gorgulho, *J. Braz. Chem. Soc.* **2006**, *17*, 1133–1143.
[52] H. F. Gorgulho, J. P. Mesquita, F. Gonçalves, M. F. R. Pereira, J. L. Figueiredo, *Carbon* **2008**, *46*, 1544–1555.
[53] Â. C. Apolinário, A. M. T. Silva, B. F. Machado, H. T. Gomes, P. P. Araújo, J. L. Figueiredo, J. L. Faria, *Appl. Catal. B* **2008**, *84*, 75–86.
[54] J. H. Ramirez, C. A. Costa, L. M. Madeira, G. Mata, M. A. Vicente, M. L. Rojas-Cervantes, A. J. López-Peinado, R. M. Martín-Aranda, *Appl. Catal. B* **2007**, *71*, 44–56.
[55] R. P. Rocha, J. P. S. Sousa, A. M. T. Silva, M. F. R. Pereira, J. L. Figueiredo, *Appl. Catal. B* **2011**, *104*, 330–336.
[56] L. Yang, L. Liu, B. A. Olsen, M. A. Nussbaum, *J. Pharm. Biomed. Anal.* **2000**, *22*, 487–493.
[57] W. C. Ketchie, Y. Fang, M. S. Wong, M. Murayama, R. J. Davis, *J. Catal.* **2007**, *250*, 94–101.
[58] ISO 6332:1988, **1988**.

Received: January 31, 2016
Revised: March 29, 2016